Hindawi Publishing Corporation
Journal of Nanomaterials
Volume 2013, Article ID 462540, 9 pages
http://dx.doi.org/10.1155/2013/462540

Research Article

Size-Controlled Synthesis of $CoFe_2O_4$ Nanoparticles Potential Contrast Agent for MRI and Investigation on Their Size-Dependent Magnetic Properties

Fujun Liu,[1] Sophie Laurent,[1] Alain Roch,[1] Luce Vander Elst,[1] and Robert N. Muller[1,2]

[1] *Department of General, Organic and Biomedical Chemistry, NMR and Molecular Imaging Laboratory, University of Mons, 7000 Mons, Belgium*
[2] *Center for Microscopy and Molecular Imaging (CMMI), Académie Wallonie, Bruxelles, 6041 Charleroi-Gosselies, Belgium*

Correspondence should be addressed to Robert N. Muller; robert.muller@umons.ac.be

Received 6 June 2013; Revised 17 September 2013; Accepted 25 September 2013

Academic Editor: Miguel A. Correa-Duarte

Cobalt ferrite nanoparticles ($CoFe_2O_4$ NPs) were synthesized by coprecipitation followed by treatments with diluted nitric acid and sodium citrate. Transmission electron microscope (TEM) and photon correlation spectroscopy (PCS) characterization showed that the size distributions of these nanoparticles were monodisperse and that no aggregation occurred. This colloid showed a long-term stability. Through adjustment of the concentrations of reactants and reaction temperature, the size of the NPs can be tuned from 6 to 80 nm. The size-control mechanism is explained by a nucleation-growth model, where the local concentration of monomers is assumed to decide the size of nuclei, and reaction temperatures influence the growth of nuclei. Magnetization and relaxivity $r_{1,2}$ measurements showed that the NPs revealed size-dependent magnetization and relaxivity properties, which are explained via a "dead magnetic layer" theory where reductions of saturation magnetization (Ms) and $r_{1,2}$ are assumed to be caused by the demagnetization of surface spins.

1. Introduction

The development of uniform magnetic nanoparticles (MNPs) has been intensively pursued for their scientific and technological importance [1–3]. The synthesis of MNPs with average sizes from 2 to 50 nm is of significant importance because of their applications in several fields, especially in biomedicine for magnetic resonance imaging (MRI) [4, 5], cell labelling [6, 7], and drug delivery [8–11]. Of special interest are their magnetic properties in which the differences between a massive or bulk material and a nanoscaled one are especially pronounced. The magnetic properties are particularly sensitive to the particle size, which is determined by the finite size effects (related to the reduced number of spins cooperatively linked within the particle), and by surface effects (greater as the particle size decreases) [12–15]. The water solubility of MNPs is necessary for medical applications, and their aggregation, caused by the huge specific surface area and magnetic interactions, must be avoided. It is thus necessary to adopt methods to stabilize the MNPs, either by using surfactants or by changing their surface potential.

Oleic acid and oleylamine are the surfactants most used for the synthesis of MNPs in organic solvent [16–19] and citric acid for water phase synthesis [20–23], as these capping agents tend to be absorbed on the particular high-energy facets. Their overall specific surface energy is more or less reduced, so the tendency towards aggregation is decreased. The ratio between growth rates in different directions can be varied by special adsorption of organic surfactants onto particular crystallographic facets specially inhibiting the growth and also the possible aggregation. On the other hand, the stability of MNPs can also be achieved by changing their surface potential [24–27], by introducing an electric repulsive force between NPs.

The general chemical formula of spinel ferrite is MFe_2O_4 (M = Fe, Mn, Co, Mg, Zn, Ni, etc.). It has a face-centered cubic (fcc) structure with a large unit cell including eight formula units. There are two kinds of lattices for cation occupancy:

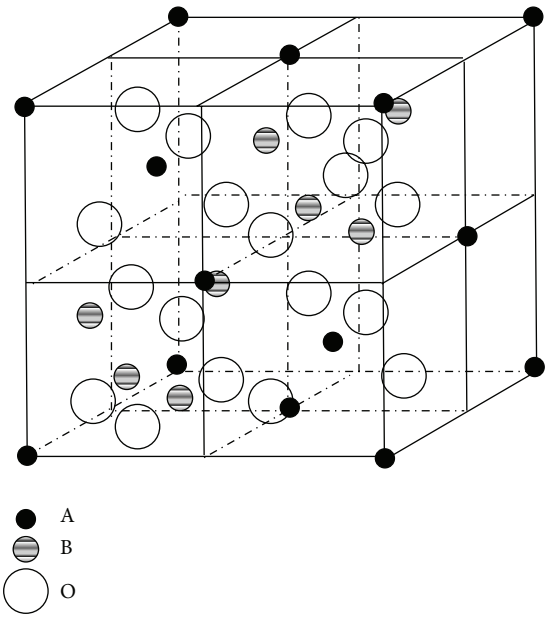

Figure 1: A schematic description of spinel MFe_2O_4, where A and B represent tetrahedral and octahedral coordination for cation occupancy, respectively [28].

tetrahedral and octahedral, which are denoted as A and B sites, respectively (see Figure 1). Spinels with only M^{2+} ions occupying A or B sites are called direct (or called normal) or inverse, respectively [28].

Among MFe_2O_4 NPs, cobalt ferrite ($CoFe_2O_4$) recently attracted interest due to its higher magnetization and r_2 proton relaxivity than magnetite (Fe_3O_4) which is mostly used as T_2 MRI contrast agent [29]. $CoFe_2O_4$ has a partially inverse spinel structure with the formula $[Co_xFe_{1-x}][Co_{1-x}Fe_{1+x}]O_4$, where the first and second square brackets indicate A and B sites, respectively. The ratio, ${Fe^{3+}}_A/{Fe^{3+}}_B$, has been found to vary from 0.61±0.04 to 0.87±0.04 for extremes-quenched and slowly cooled samples [30, 31], respectively. For both ionic distributions, a magnetic moment of more than 3 μ_B per unit chemical formula or 71.5 $Am^2\,kg^{-1}$ is anticipated assuming 5 μ_B for Fe^{3+} and 3 μ_B for Co^{2+} ions (as Fe^{2+} ions are assumed to be 4 μ_B, the total moment of Fe_3O_4 and γ-Fe_2O_3 per formula unit is anticipated to be 4 and 2.5 μ_B, resp., and the experimental values vary with different synthetic methods [32, 33]). The observed values, 3.4 μ_B for extremes-quenched samples and 3.9 μ_B for slowly cooled samples, respectively, confirmed this expectation. There have been many reports on synthesis of $CoFe_2O_4$ NPs by different methods. Davies et al. have reported the preparation of $CoFe_2O_4$ NPs with sizes of about 3 nm by coprecipitation method [34], which exhibited multiaxial anisotropy. The value of the magnetic anisotropy constant calculated from measurements of the decay of remanence was similar to that reported for bulk cobalt ferrite. Moume and coworkers have prepared $CoFe_2O_4$ NPs with sizes of about 5 nm by the inverse micellar process [35].

To our knowledge, very little work has been done on size-controllable synthesis of $CoFe_2O_4$ NPs. Recently, it has been reported that the magnetic and relaxivity properties are dependent on the size of NPs [4]. Here $CoFe_2O_4$ NPs were obtained by coprecipitation, and the size-controlling factors were studied during the synthesis process, as well as the stabilizing effects of both citrates as the capping agents and dilute nitric acid solution to change the surface potential of NPs.

2. Materials and Methods

2.1. Materials. Distilled water was used to prepare all aqueous solutions. Ferric chloride hexahydrate ($FeCl_3{\cdot}6H_2O$), cobalt chloride hexahydrate ($CoCl_2{\cdot}6H_2O$), sodium citrate, 1, 10-phenanthrolin (99%), and hydroxylamine hydrochloride ($NH_2OH{\cdot}HCl$) were purchased from Sigma Chemical (Bornem, Belguim). All other reagents and solvents were purchased from Aldrich Chemical (Bornem, Belguim) and were of the highest grade commercially available.

2.2. Methods. 1 mL of 20 M NH_4OH was added dropwise to the solution mixture of 20 mL of 2 M $FeCl_3{\cdot}6H_2O$ and 1 M $CoCl_2{\cdot}6H_2O$ in 0.4 M HCl (denoted as (Co+Fe)) with constant stirring, at 80°C. The precipitation occurred immediately, turning the color of the reaction suspension into dark brown. During the precipitation, the reaction mixture was vigorously stirred for 2 h at desired temperature. The resulting precipitates were separated by a permanent magnetic field and washed with distilled water and the separation/washing processes were repeated 5 times until the washed water was free of chloride ions. The washed samples were dispersed in 20 mL 0.02 M HNO_3 solution and stirred for 1 h at 80°C, followed by adding 0.8 g sodium citrate and stirring for another 4 h. Centrifugal filter units (Millipore, 10k MWCO) were used to purify the samples and remove the unabsorbed H^+ and citric ions.

2.3. Instrumentation. TEM images were collected on a Tecnai 10 (FEI, Hillsboro, USA) with operating voltage at 200 kV. IR spectra were obtained on a Spectrum 100 Series (Perkin Elmer, Massachusetts, USA) spectrometer in ATR mode. The hydrodynamic size and surface potential of $CoFe_2O_4$ NPs were measured on Zetasizer Nano Series Zen 3600 (Malvern, Worcestershire, United Kingdom), into which 1 mL sample solution of about 2 mM was put in the cell and measured at 37°C.

As there were peak overlaps between Fe and Co absorption for inductively coupled plasma (ICP) measurements, the concentration of Fe was confirmed by spectrometry, using 1,10-phenanthrolin as the chromogenic agent, and the concentration of Co was obtained through the external standard method by measuring the R_1 values, for which the detailed process is described in supplementary in supplementary material available online at http://dx.doi.org/10.1155/2013/462540.

The stability of the NPs was evaluated using a Turbiscan optical analyzer (Formulaction SA, L'Union, France), an innovative analytical instrument able to determine the long-term stability of colloidal systems. 15 mL sample colloid was placed into a cylindrical glass tube and submitted to

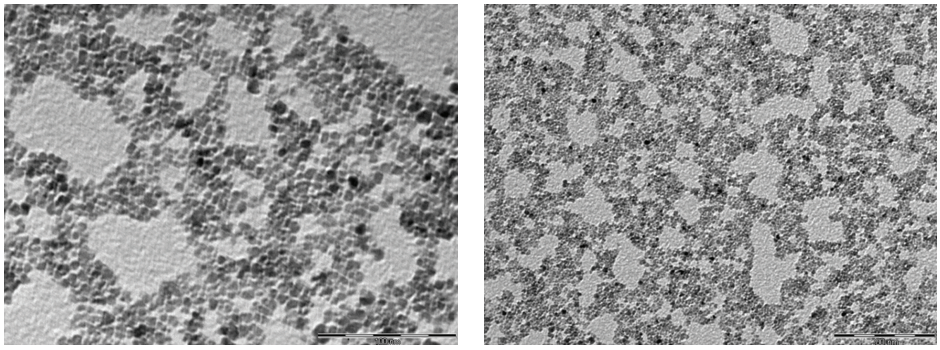

(a) (b)

Figure 2: TEM picture of obtained $CoFe_2O_4/H^+$/citrate NPs with a diameter by PCS being 28.35 nm, where the scale bars for (a) and (b) are 100 nm and 200 nm, respectively. The TEM diameter and polydispersity index (PDI) are 10.38 nm and 1.1017, respectively, calculated by the software iTEM (Olympus, Tokyo, Japan).

Turbiscan Lab Expert stability analysis. The measurements were carried out at 37 ± 2°C for 24 h at intervals of 1 h.

To study the magnetic properties of the NPs obtained, magnetic hysteresis curves were obtained by VSM-NUVO (Molspin Ltd., Newcastle-on-Tyne, England), r_1/r_2 were measured on MiniSpec mq-20 (20 MHz) and mq-60 (60 MHz) (Bruker, Ettlingen, Germany), and nuclear magnetic relaxation dispersion (NMRD) profiles were performed on Spinmaster-FFC 2000 relaxometer (Stelar SRT, Mede, Italy).

3. Results and Discussion

3.1. Preparation and Size Controlling of $CoFe_2O_4$ NPs. The reaction to synthesize $CoFe_2O_4$ NPs can be described by

$$\begin{aligned} &CoCl_2 + 2FeCl_3 + n NH_4OH \\ &\longrightarrow CoFe_2O_4 + (n-8)\,NH_4OH + 4H_2O + 8NH_4Cl \end{aligned} \quad (1)$$

where the variable $n \geq 8$ stands for the relative amount of NH_4OH. The total concentration of Co^{2+} and Fe^{3+} is denoted by $[Co^{2+} + Fe^{3+}]$, and the concentration of OH^- is denoted by $[OH^-]$. By adjusting n, the ratio $[Co^{2+} + Fe^{3+}] : [OH^-]$ (denoted by x, where $x = 3/n$) varied from 0.00625 to 0.1. The average diameter of $CoFe_2O_4$ NPs can be tuned from 13 to 38 nm, by varying the reaction parameters, such as feeding order, reactant concentrations and pH value. Figure 2 shows the TEM pictures of $CoFe_2O_4$ NPs after treatment with diluted nitric acid and sodium citrate (denoted as $CoFe_2O_4/H^+$/citrate with the hydrodynamic diameter (measured by PCS, denoted as D_{PCS}) of 28.35 nm). The TEM picture agrees with monodisperse particles as confirmed by the corresponding statistics graphs using PCS (see Figures S3 and S4).

During the process of drying samples on carbon-coated copper grids, several NPs were adsorbed onto each other, which look like "aggregations" in Figure 2. To clearly prove the absence of aggregations, sizes of $CoFe_2O_4$ NPs measured by different methods are compared in Table 1. Although various methods (VSM, TEM, NMRD, and PCS) are available, the accuracy of the results for NPs sizes is not always clear because of possible systematic errors of the analysis. Each technique has its own advantage and disadvantage. TEM is certainly the most direct method, providing real images of the particles, which can be considered as an essential tool to get an impression of the homogeneity of given samples, but the lack of contrast or overlap of particles complicates the TEM image analysis. The technologies of VSM and PCS are both based on indirect calculations. The calculation of NPs sizes by VSM is based on the Langevin curve fitting as follows:

Table 1: Diameters of $CoFe_2O_4/H^+$/citrate NPS measured by different methods for five different samples (denoted as SP1, SP2, SP3, SP4. and SP5).

Sample	D_{VSM}/nm	D_{TEM}/nm	D_{PCS}/nm
SP1	4.61	7.25	12.98
SP2	5.53	8.51	15.97
SP3	5.90	9.26	19.25
SP4	6.13	10.38	28.35
SP5	7.04	11.02	37.89

$$\mathrm{ma}\left(B_o\right) = MsL\left(x\right), \quad (2)$$

where $\mathrm{ma}(B_o)$ is the magnetization of the suspension at a field B_o, Ms is the magnetization at saturation, and $L(x)$ is the Langevin function (3)

$$L\left(x\right) = \left[\coth\left(x\right) - \frac{1}{x}\right] \quad \text{with } x = \frac{Ms\left(T\right)VB_o}{kT}, \quad (3)$$

where k and T are the Boltzmann constant and the absolute temperature, respectively, and the fitting process will be described subsequently [4]. PCS is based on a time-dependent fluctuation in the scattering intensity, as the source light hits small particles and the light scatters in all directions (Rayleigh scattering) so long as the particles are small compared to the wavelength (below 250 nm). The size value obtained by PCS is the hydrodynamic diameter of a sphere, which may be larger than that from TEM due to the presence of surfactants or coating molecules. As shown in

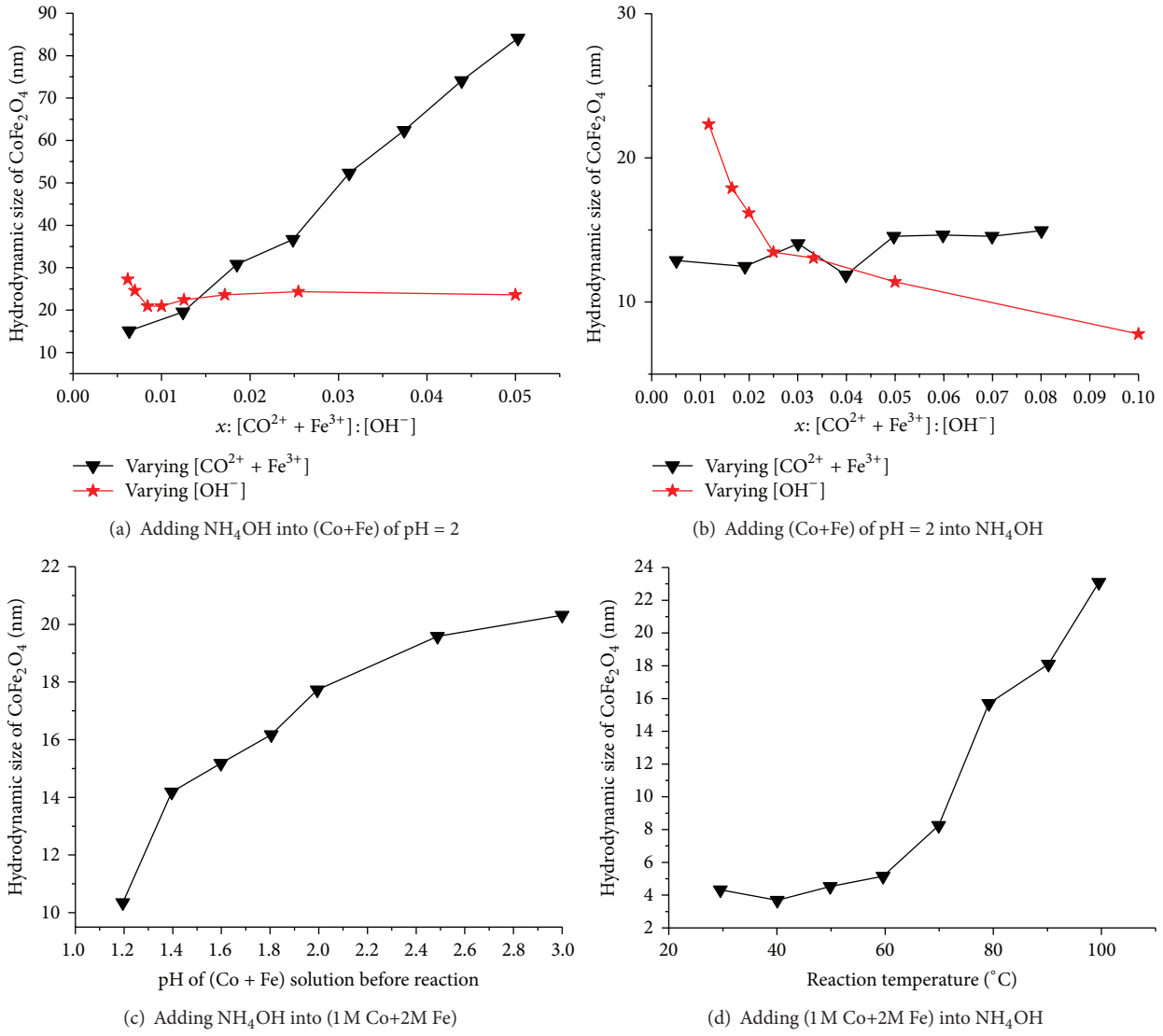

FIGURE 3: Control of the sizes of $CoFe_2O_4$/H^+/citrate NPs by varying different parameters. The feeding orders of (a) and (b) were adding NH_4OH into (Co+Fe) and adding (Co+Fe) into NH_4OH, respectively, and the red/black line represented the results of varying $[Co^{2+}+Fe^{3+}]/[OH^-]$; (c) and (d) show the change of $CoFe_2O_4$ NPs sizes by adjusting the pH of (Co+Fe) and the reaction temperature, respectively.

Table 1, the diameter values obtained by VSM, TEM, and PCS are denoted by D_{VSM}, D_{TEM}, and D_{PCS}, respectively. D_{PCS} for each sample is much bigger than D_{VSM}, and D_{TEM}, because of the absorbed citrate layer.

It has been found that the values of some parameters experimented will affect the particle size and morphology [29, 38]. The following parameters were varied: the value of x, the reaction temperature, and the pH (see Figure 3). It was found that the NPs size is very sensitive to the ratio x with adjustment of $[Co^{2+} + Fe^{3+}]$, as shown in Figure 3(a). To systemically investigate the influence of x on the size, $[Co^{2+} + Fe^{3+}]$ or $[OH^-]$ was changed for different feeding orders: adding NH_4OH into (Co + Fe) or adding (Co + Fe) into NH_4OH, as shown in Figures 3(a) and 3(b), respectively. Increasing x induced completely opposite effects on the final sizes of $CoFe_2O_4$ NPs depending on the feeding orders. When NH_4OH is added into (Co + Fe) (see Figure 3(a)), the increase of x caused by varying $[Co^{2+} + Fe^{3+}]$ (the line with triangle symbols) results in a linear increase of the hydrodynamic size of the NPs from 15 to 80 nm, whereas varying $[OH^-]$ (the line with star symbols) does not influence the NPs sizes (the size is about 22 nm, regardless of the value of x). On the other hand, when the (Co + Fe) mixture was added into the NH_4OH solution (see Figure 3(b)), NPs sizes decreased from 22 to 7 nm as $[OH^-]$ decreased (increasing x), but remained constant (about 17 nm) when $[Co^{2+} + Fe^{3+}]$ was varied. Such a phenomenon had never been previously reported and can be explained as described hereafter.

It is well known that the formation of NPs can be divided into two-step processes: nucleation initiated by a sudden increase of monomer concentration up to super-saturation levels and subsequent growth of nuclei with progressive

consumption of monomers in reaction medium (see Figure S5) [39]. The final geometrical properties of NPs are determined by several parameters during the nucleation and growth processes. During the coprecipitation of Co^{2+} and Fe^{3+} into $CoFe_2O_4$, when the drop of added solution (denoted by Sol_A, as the green solution in a pipette in Figure S5) comes into contact with the initial solution (denoted by Sol_B, as the yellow solution in a beaker in Figure S5), the reaction of (1) is initiated immediately to form $CoFe_2O_4$ monomers. As a consequence, the local concentration of monomers suddenly reaches saturation ($c_{sat.}$) and then the super-saturation state, followed by the nucleation and growth processes. In such a classical ionic reaction, Sol_A is at a high concentration (and small volume) to make sure that the total volume of the reaction system does not change too much. So the amount and concentration of monomers formed mainly depend on Sol_B which is at a lower concentration.

The above hypothesis explains why only the concentration of Sol_B influences the size of $CoFe_2O_4$ NPs, no matter whatkind of feeding order is adopted. When adding NH_4OH into the (Co + Fe) mixture solution, $[OH^-]$ is much larger than $[Co^{2+} + Fe^{3+}]$, so only the increase of $[Co^{2+} + Fe^{3+}]$ (Sol_B) can result in bigger $CoFe_2O_4$ NPs, and the change of $[OH^-]$ (Sol_A) does not influence the size of NPs. On the other hand, when adding the (Co + Fe) mixture into NH_4OH, the size of NPs decreases with lowering $[OH^-]$ (Sol_B) but remains constant with changing $[Co^{2+} + Fe^{3+}]$ (Sol_A). This means that NPs sizes do not dependent on the ratio between $[Co^{2+} + Fe^{3+}]$ and $[OH^-]$ but depend on the concentration of monomers. To confirm this hypothesis, HCl was used to adjust the pH of the Co + Fe mixture, when NH_4OH was added to this mixture. The results show that NPs size increases as the pH increases (see Figure 3(c)). The reason should be that the protons in the Co + Fe mixture react with the OH^- of the NH_4OH solution. Hence the local concentration of NH_4OH (Sol_B) is decreased and smaller NPs are obtained. It had been reported by Lee et al. that the size and structure of nuclei were the key to deciding the final size of obtained NPs [40]. Consequently, a higher local concentration of monomers leads to larger nuclei and thus increases the size of final NPs.

The influence of the reaction temperature was studied and the results are shown in Figure 3(d). The NPs sizes become larger as the temperature increased. This phenomenon matches with literature reports showing that high temperature contributes to the growth of nuclei to obtain large NPs [41].

3.2. Stabilization of $CoFe_2O_4$ NPs. Li et al. reported that acidic treatment on $CoFe_2O_4$ NPs resulted in a noncrystalline porous wrapping layer on the surface and in the constituting of coated bodies [42]. Here the stability of $CoFe_2O_4$ NPs treated with diluted nitric acid (denoted by $CoFe_2O_4/H^+$) and NPs only treated by sodium citrate (denoted as $CoFe_2O_4$/citrate) were compared after dispersion in water and being left at room temperature. $CoFe_2O_4$/citrate suspension was found to deposit in about 0.5 h, while $CoFe_2O_4/H^+$ remains stable for more than 2 months, without any sedimentation. To further test the stability of $CoFe_2O_4/H^+$, a strong magnetic field was applied (see Figure 4). It was found that $CoFe_2O_4$ without any treatment and $CoFe_2O_4$/citrate NPs were easily separated by magnetic force, but that $CoFe_2O_4/H^+$ suspension kept stable. After nitric acid treatment for 1 h, sodium citrate was added and stirring was continued for another 4 h. The obtained NPs, denoted by $CoFe_2O_4/H^+$/citrate, are kept stable under magnetic field like $CoFe_2O_4/H^+$ (not shown). D_{PCS} of $CoFe_2O_4$, $CoFe_2O_4$/citrate, $CoFe_2O_4/H^+$, and $CoFe_2O_4/H^+$/citrate measured by PCS was 1100, 600, 12 and 13 nm, respectively. Because of their ultrasmall size, $CoFe_2O_4/H^+$ and $CoFe_2O_4/H^+$/citrate NPs have no obvious response to an applied magnetic field and the electrostatic repulsion force also contributes to keeping the suspension stable. Figure S6 gives the IR spectra of $CoFe_2O_4$/citrate and $CoFe_2O_4/H^+$/citrate NPs. The peaks at 3392, 2905, 2850, 1587, and 1379 cm^{-1} are vibration modes of sym(OH), asy(CH_2), sym(CH_2), asy(CO_2), and sym(CO_2), respectively. The spectrum demonstrates the successful attachment of sodium citrate onto the surface of $CoFe_2O_4/H^+$/citrate because the characteristic absorption peaks of sodium citrate at 3392, 1587, and 1379 cm^{-1} are strong (the black curve in Figure S6), whereas these peaks are weak for $CoFe_2O_4$/citrate (the red curve in Figure S6). Sodium citrate was thus not effectively anchored on the $CoFe_2O_4$ NPs surface and there were aggregations as well, according to Figure 4(b). This can be explained by the fact that the acidic treatment induces etching of the bigger particles or aggregations as well as other single smaller particles, thus forming porous viscous layers on their surface, where sodium citrate can be adsorbed.

To investigate the long-term stability of the $CoFe_2O_4/H^+$/citrate colloid, the sample was tested by both its optical transmission and photon backscattering properties. The principle of this measurement is based on

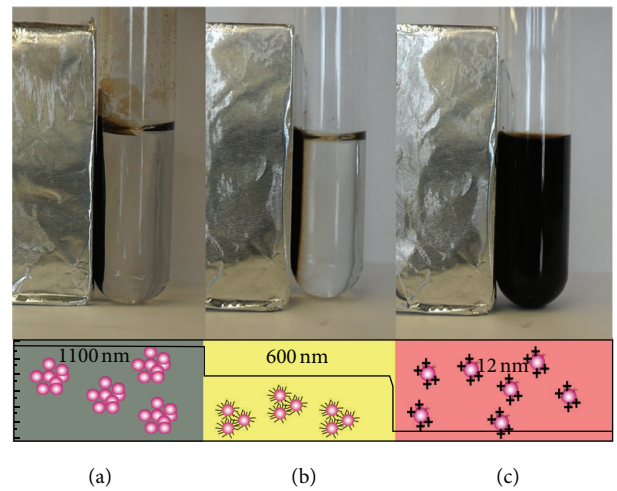

FIGURE 4: Photographs of $CoFe_2O_4$ NPs suspensions, (a) without any treatment, (b) treated only by sodium citrate and (c) treated by dilute HNO_3 solution. The lower figure shows the size values obtained by PCS for each sample.

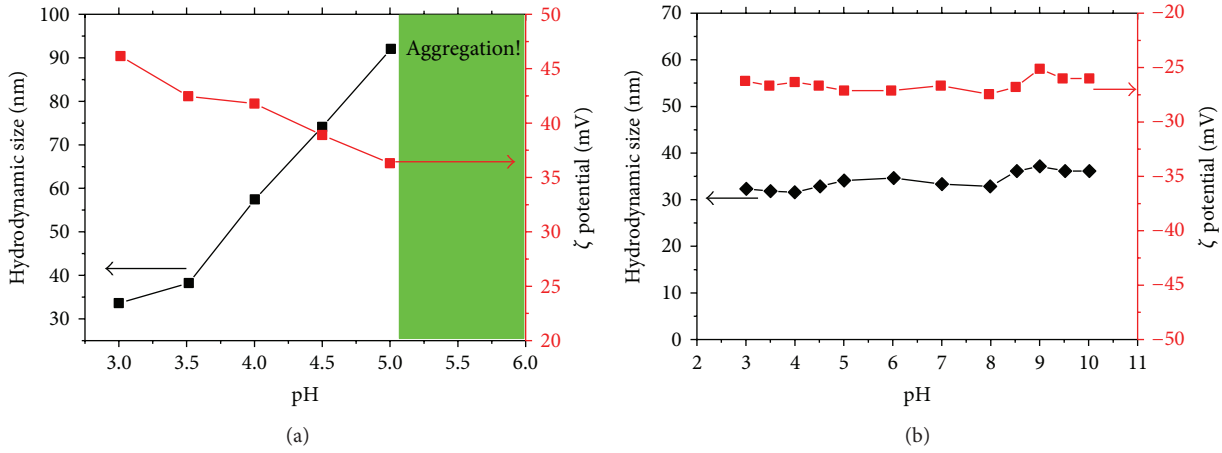

FIGURE 5: Zeta potential and hydrodynamic size of $CoFe_2O_4$ NPs at different pH values, (a) $CoFe_2O_4/H^+$ (SP3 before citrate treatment) and (b) $CoFe_2O_4/H^+$/citrate (SP3).

the variation of the droplet volume fraction (migration) or mean size (coalescence), which results in the variation of backscattering and transmission signals. The backscattering signal will show change as a function of time if particle migration occurs and is graphically reported in the form of positive (backscattering increase) or negative peaks (backscattering decrease). In fact, the migration of particles from the top to the bottom of a sample leads to a progressive concentration decrease at the top of the sample, which causes an increase in the backscattering signal (positive peak) and a decrease in the intensity of the transmission (positive peak). Such changes will be affected if aggregation of particles occurs [43–45].

The transmission and backscattering profiles of $CoFe_2O_4/H^+$/citrate colloid (D_{PCS} = 37.89 nm) are shown in Figure S7. The backscattering profile being within the interval ±2% means that no variation of particle size occurs during measurements. Variations of backscattering profile (ΔBS) greater than 10% (either positive or negative value) are representative of an unstable system. In Figure S7, the curves between 5 and 30 mm (bracketed by red dashed lines) represented transmission and backscattering intensions of colloid parts. ΔBS was found within the interval ±2% during 24 h, which proved that no variation of particle size occurred and this $CoFe_2O_4$ colloid was stable. Other $CoFe_2O_4$ samples showed similar results (not shown here), confirming that NPs obtained by our strategy are stable and that no aggregation occurs.

To investigate the stability of $CoFe_2O_4$ NPs in medium with different pH values, the sizes and zeta potentials of $CoFe_2O_4/H^+$ NPs and $CoFe_2O_4/H^+$/citrate (see Figure 5) were studied. As shown in Figure 5(a), with increasing pH from 3 to 5, the hydrodynamic size of acid treated $CoFe_2O_4$ NPs increased from 34 to 90 nm. In acid medium, there is an equilibrium between the adsorption and desorption of H^+ ions on the surface of $CoFe_2O_4$ NPs. When increasing the pH, lower $[H^+]$ in the medium led to more desorption of H^+ ions on the surface of NPs and decreased the electrostatic repulsion, which caused the aggregation and enlarged the size of NPs. It was furthermore confirmed by the study of zeta potential (the red curve in Figure 5(a)) that the surface of acid treated $CoFe_2O_4$ NPs was positively charged in acidic medium, and the zeta value decreased from 46 to 36 mV as the pH increased. At pH > 5, the aggregation was too high and caused deposition of NPs. On the other hand, the size and zeta potential of $CoFe_2O_4/H^+$/citrate remain constant (about 33 nm and −27 mV, resp., in the pH region of 3–10) (see Figure 5(b)). As discussed above, acidic treatment makes NPs surfaces positively charged and forms porous viscous layers, where citrate can be adsorbed. The adsorbed citrate turns NPs surface from being positively to negatively charged, which has a stable zeta potential over the pH range.

3.3. Magnetic Properties of $CoFe_2O_4$ NPs. Magnetic measurements were carried out at room temperature on aqueous suspensions of $CoFe_2O_4/H^+$/citrate NPs with different D_{PCS}. The fitting of the experimental magnetization data (see Figure 6) by (2) and (3) allows for the determination of the crystal size and its *Ms*. The lack of hysteresis (almost zero coercive force, Hc) and remanence at ambient temperatures is characteristic of superparamagnetic materials. The specific magnetization is the magnetic moment per unit mass. In this paper, magnetizations are reported with respect to the total mass of iron and cobalt (i.e., Am^2/kg Fe + Co). The results (see Figure 6) indicate that the saturation magnetization, *Ms*, increases from 28.42 to 45.50 $Am^2\,kg^{-1}$, as D_{PCS} increases from 12.98 to 37.89 nm. The size-dependent change of *Ms* has already been observed in some small particle systems [46]. This can be explained by postulating the existence of a "dead magnetic" layer due to the demagnetization of the surface spins when the size of the sample is in nano-region, which causes a reduction of *Ms* [47]. The ratio of surface to volume is inversely proportional to the particle size. As the particle gets smaller, surface molecules make up greater shares, which leads to more "dead magnetic" components. So as the particle size decreases, the proportion of "dead magnetic" components increases and *Ms* decreases.

The efficacy of NPs as contrast agent for MRI is related to their r_1 and r_2 relaxivity values (Table 2). Relaxivities are

Table 2: T_1 and T_2 relaxivities ($r_1$and r_2, resp.) measurements on $CoFe_2O_4/H^+$/citrate NPs with different D_{PCS}, where the last two samples Feridex and Resovist are used as references.

D_{PCS}/nm	Relaxivity at 20 MHz			Relaxivity at 60 MHz		
	r_1 /$s^{-1}mM^{-1}$	r_2 /$s^{-1}mM^{-1}$	r_2/r_1	r_1 /$s^{-1}mM^{-1}$	r_2 /$s^{-1}mM^{-1}$	r_2/r_1
12.98	12.8	16.6	1.3	7.1	12.4	1.75
15.97	16.6	39.8	2.4	7.9	34.8	4.4
19.25	24.1	55.4	2.3	9.7	49.5	5.1
28.35	26.9	69.9	2.6	10	52	5.2
37.89	27.8	75.1	2.7	9.1	51	5.6
Feridex [36]	40	160	4	—	—	—
Resovist [37]	25	164	6.2	—	—	—

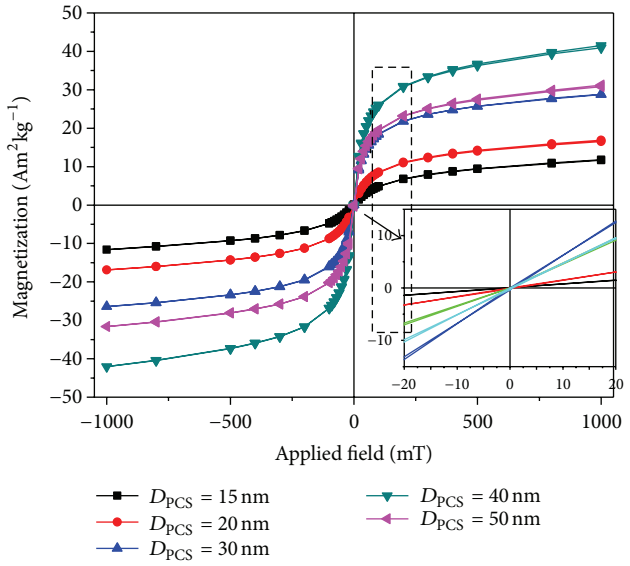

Figure 6: Magnetization versus applied field curves of $CoFe_2O_4$ NPs with different hydrodynamic diameters. The inset shows the non-hysteresis of $CoFe_2O_4$ NPs.

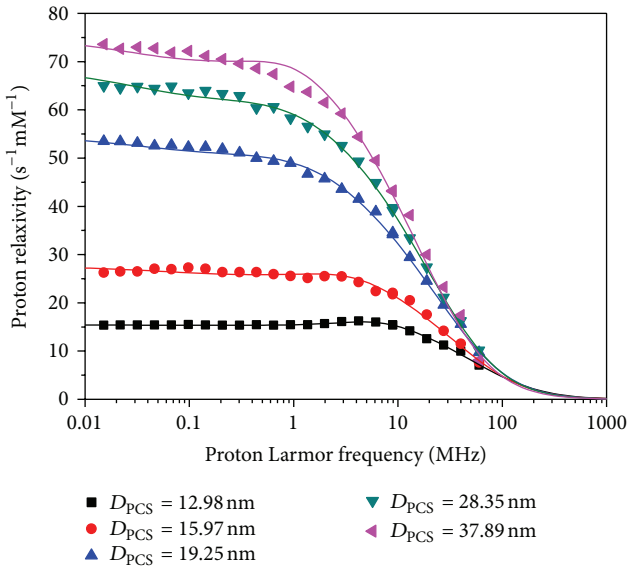

Figure 7: NMRD profiles of samples with different hydrodynamic sizes (relaxivity is the water proton relaxation rate increase induced by a concentration of 1 mM of iron and cobalt in the solution), accompanied by corresponding fitting results.

reported with respect to the total molarity of iron and cobalt (i.e., $s^{-1}\,mM^{-1}$ Fe + Co). The values of r_2 (related to T_2 contrast) increase with particle diameters at 20 and 60 MHz. When D_{PCS} of $CoFe_2O_4/H^+$/citrate NPs increases from 12.89 to 37.89 nm, the values of r_2 at 20 MHz increase sharply from 16.6 to 75.1 s^{-1} mM^{-1}. r_2 values of NPs with D_{PCS} larger than 60 nm cannot be accurately measured because of their aggregation in the presence of a magnetic field. This size dependence is believed to arise from surface spin anisotropy, which is more pronounced for smaller particles due to larger surface area to volume ratios. As the NPs are superparamagnetic, the transverse relaxivity rate r_2 is enhanced due to rapid diffusion and exchange of surrounding water molecules. In such a "motion averaging regime" (MAR) [48], it is postulated that the $CoFe_2O_4$ contrast agents are homogenously distributed and the diffusion of surrounding water molecules to and from the surface layer of superparamagnetic cores occurs in faster time scales than proton magnetic relaxation.

Similar phenomena were found in the NMRD measurements. Obtained curves give the R_1 relaxivity evolution versus the external magnetic field, where the relaxivity is defined as the increase of the R_1 relaxation rate of the solvent (H_2O) induced by 1 mmol/L of the active iron and cobalt ions. The spin lattice relaxation profiles of the above $CoFe_2O_4$ NPs are shown in Figure 7. In general, for magnetic NPs colloids, the shape of the NMRD profile is determined by (i) the size and crystallinity of magnetic cores, as they affect the *Ms*; (ii) the accessibility of the cores to the diffusing solvent molecules; and (iii) interactions between cores, as they affect the anisotropy energy [4]. The size effect is known to be a potentially strong contributor in low frequency range in particular. The NMRD data demonstrate that increasing NPs sizes produced systematic changes in the magnetic resonance properties of the colloids, particularly in the low-frequency (sub MHz) part of the profiles, where values of r_1 increase as

Table 3: Saturation magnetization (Ms) and diameter (D_{NMRD}) obtained by fitting the NMRD files in Figure 7, where Ms_{NMRD}/$Am^2\,kg^{-1}$ and Ms_{VSM}/$Am^2\,kg^{-1}$ are the fitted Ms results from NMRD and VSM measurements, respectively.

D_{PCS}/nm	12.98	15.97	19.25	28.35	37.89
Ms_{NMRD}/Am^2kg^{-1}	35.8	36.6	38.6	41.3	41.5
Ms_{VSM}/Am^2kg^{-1}	28.42	30.93	38.95	41.09	45.5
D_{NMRD}/nm	4.81	5.77	6.82	7.44	8.3
D_{VSM}/nm	4.61	5.53	5.90	6.13	7.04
D_{TEM} /nm	7.25	8.51	9.26	10.38	11.02

the diameter of NPs increases. All samples show characteristic superparamagnetic behavior, as their Larmor frequencies present continuous decreasing trends in the high-frequency part and the corresponding fitting lines coincide well with the superparamagnetic model, and the magnetization saturation and particle diameters obtained by the fitting, as well as those obtained in the above VSM fitting, are listed in Table 3. As both kinds of fittings are based on the Langevin function, the values of Ms and particle diameters obtained by fittings of NMRD profiles and VSM data are quite similar.

4. Conclusions

In summary, the present work demonstrates a facile approach to the size-controllable preparation of superparamagnetic $CoFe_2O_4$ NPs by coprecipitation. Using different feeding orders, it was found that only the low-concentration solution has influence on the size of NPs. By a novel model, it was presumed that local concentration of monomers decided the size of nuclei in the nucleation process, and the temperature influences the growth of nuclei.

In addition to playing a role in stabilizing, acidic treatment also formed porous viscous layers on particle surface, where sodium citrate could be absorbed. The adsorbed citrate turned NPs surface from positive to negative charged, resulting in an NPs colloid solution stable over a wide pH range.

The prepared $CoFe_2O_4$ NPs showed size-dependent magnetization and proton relaxivity, which can be explained with a "dead magnetic" layer model. The surface spin anisotropy induces decreases in Ms and $r_1/2$ for smaller particles. Furthermore, this facile synthetic procedure may be widely applied in size-controllable synthesis of mono- metallic or multi-metallic oxides by using different metallic cations.

Conflict of Interests

The authors declare that there is no conflict of interests.

Acknowledgments

This work was supported by the Fonds de la Recherche Scientifique, the ARC Program 05/10-335 of the French Community of Belgium, and the ENCITE program of the European Community. The support and sponsorship concerted by COST Action D38 "Metal-Based Systems for Molecular Imaging Applications" and the EMIL program are kindly acknowledged. The authors are grateful to Dr. Yves GOSSIUN in UMons for performing VSM analysis and to Dr. David PEREZ-MORGA for the TEM analysis.

References

[1] S. A. Majetich and Y. Jin, "Magnetization directions of individual nanoparticles," *Science*, vol. 284, no. 5413, pp. 470–473, 1999.

[2] H. Zeng, J. Li, J. P. Liu, Z. L. Wang, and S. Sun, "Exchange-coupled nanocomposite magnets by nanoparticle self-assembly," *Nature*, vol. 420, no. 6914, pp. 395–398, 2002.

[3] C. Thirion, W. Wernsdorfer, and D. Mailly, "Switching of magnetization by nonlinear resonance studied in single nanoparticles," *Nature Materials*, vol. 2, no. 8, pp. 524–527, 2003.

[4] S. Laurent, D. Forge, M. Port et al., "Magnetic iron oxide nanoparticles: synthesis, stabilization, vectorization, physicochemical characterizations and biological applications," *Chemical Reviews*, vol. 108, no. 6, pp. 2064–2110, 2008.

[5] L. Schröder, T. J. Lowery, C. Hilty, D. E. Wemmer, and A. Pines, "Molecular imaging using a targeted magnetic resonance hyperpolarized biosensor," *Science*, vol. 314, no. 5798, pp. 446–449, 2006.

[6] S. Laurent, S. Boutry, I. Mahieu, L. Vander Elst, and R. N. Muller, "Iron oxide based MR contrast agents: from chemistry to cell labeling," *Current Medicinal Chemistry*, vol. 16, no. 35, pp. 4712–4727, 2009.

[7] B. P. Barnett, A. Arepally, P. V. Karmarkar et al., "Magnetic resonance-guided, real-time targeted delivery and imaging of magnetocapsules immunoprotecting pancreatic islet cells," *Nature Medicine*, vol. 13, no. 8, pp. 986–991, 2007.

[8] M. Mahmoudi, S. Sant, B. Wang, S. Laurent, and T. Sen, "Superparamagnetic iron oxide nanoparticles (SPIONs): development, surface modification and applications in chemotherapy," *Advanced Drug Delivery Reviews*, vol. 63, no. 1-2, pp. 24–46, 2011.

[9] S. J. Son, J. Reichel, B. He, M. Schuchman, and S. B. Lee, "Magnetic nanotubes for magnetic-field-assisted bioseparation, biointeraction, and drug delivery," *Journal of the American Chemical Society*, vol. 127, no. 20, pp. 7316–7317, 2005.

[10] Q. Cao, X. Han, and L. Li, "Enhancement of the efficiency of magnetic targeting for drug delivery: development and evaluation of magnet system," *Journal of Magnetism and Magnetic Materials*, vol. 323, no. 15, pp. 1919–1924, 2011.

[11] Y. Yoshida, S. Fukui, S. Fujimoto et al., "Ex vivo investigation of magnetically targeted drug delivery system," *Journal of Magnetism and Magnetic Materials*, vol. 310, no. 2, pp. 2880–2882, 2007.

[12] W. S. Seo, H. H. Jo, K. Lee, B. Kim, S. J. Oh, and J. T. Park, "Size-dependent magnetic properties of colloidal Mn_3O_4 and MnO nanoparticles," *Angewandte Chemie: International Edition*, vol. 43, no. 9, pp. 1115–1117, 2004.

[13] T.-J. Park, G. C. Papaefthymiou, A. J. Viescas, A. R. Moodenbaugh, and S. S. Wong, "Size-dependent magnetic properties of single-crystalline multiferroic $BiFeO_3$ nanoparticles," *Nano Letters*, vol. 7, no. 3, pp. 766–772, 2007.

[14] K. N. K. Kowlgi, G. J. M. Koper, S. J. Picken, U. Lafont, L. Zhang, and B. Norder, "Synthesis of magnetic noble metal (nano)particles," *Langmuir*, vol. 27, no. 12, pp. 7783–7787, 2011.

[15] H. Duan, M. Kuang, X. Wang, Y. A. Wang, H. Mao, and S. Nie, "Reexamining the effects of particle size and surface chemistry on the magnetic properties of iron oxide nanocrystals: new insights into spin disorder and proton relaxivity," *The Journal of Physical Chemistry C*, vol. 112, no. 22, pp. 8127–8131, 2008.

[16] S. Sun, H. Zeng, D. B. Robinson et al., "Monodisperse MFe_2O_4 (M = Fe, Co, Mn) Nanoparticles," *Journal of the American Chemical Society*, vol. 126, no. 1, pp. 273–279, 2004.

[17] K. T. Wu, Y. D. Yao, and H. K. Huang, "Comparison of dynamic and optical properties of Fe_3O_4 ferrofluid emulsion in water and oleic acid under magnetic field," *Journal of Magnetism and Magnetic Materials*, vol. 209, no. 1-3, pp. 246–248, 2000.

[18] Z. Jia, J. W. Harrell, and R. D. K. Misra, "Synthesis and magnetic properties of self-assembled FeRh nanoparticles," *Applied Physics Letters*, vol. 93, no. 2, Article ID 022504, 2008.

[19] G. K. Das, B. C. Heng, S.-C. Ng et al., "Gadolinium oxide ultranarrow nanorods as multimodal contrast agents for optical and magnetic resonance imaging," *Langmuir*, vol. 26, no. 11, pp. 8959–8965, 2010.

[20] Y. Sahoo, A. Goodarzi, M. T. Swihart et al., "Aqueous ferrofluid of magnetite nanoparticles: fluorescence labeling and magnetophoretic control," *The Journal of Physical Chemistry B*, vol. 109, no. 9, pp. 3879–3885, 2005.

[21] M. Răcuciu, D. E. Creangă, and A. Airinei, "Citric-acid-coated magnetite nanoparticles for biological applications," *European Physical Journal E*, vol. 21, no. 2, pp. 117–121, 2006.

[22] D. E. Creangă, M. Culea, C. Nădejde, S. Oancea, L. Curecheriu, and M. Racuciu, "Magnetic nanoparticle effects on the red blood cells," *Journal of Physics: Conference Series*, vol. 170, no. 1, Article ID 012019, 2009.

[23] T. Goetze, C. Gansau, N. Buske, M. Roeder, P. Görnert, and M. Bahr, "Biocompatible magnetic core/shell nanoparticles," *Journal of Magnetism and Magnetic Materials*, vol. 252, no. 1-3, pp. 399–402, 2002.

[24] A. Villanueva, M. Canete, A. G. Roca et al., "The influence of surface functionalization on the enhanced internalization of magnetic nanoparticles in cancer cells," *Nanotechnology*, vol. 20, no. 11, Article ID 115103, 2009.

[25] R. Massart, "Preparation of aqueous magnetic liquids in alkaline and acidic media," *IEEE Transactions on Magnetics*, vol. 17, no. 2, pp. 1247–1248, 1981.

[26] F. A. Tourinho, R. Franck, and R. Massart, "Aqueous ferrofluids based on manganese and cobalt ferrites," *Journal of Materials Science*, vol. 25, no. 7, pp. 3249–3254, 1990.

[27] J.-C. Bacri, R. Perzynski, D. Salin, V. Cabuil, and R. Massart, "Ionic ferrofluids: a crossing of chemistry and physics," *Journal of Magnetism and Magnetic Materials*, vol. 85, no. 1-3, pp. 27–32, 1990.

[28] J. F. Hochepied, P. Bonville, and M. P. Pileni, "Nonstoichiometric zinc ferrite nanocrystals: syntheses and unusual magnetic properties," *The Journal of Physical Chemistry B*, vol. 104, no. 5, pp. 905–912, 2000.

[29] V. F. Puntes, K. M. Krishnan, and A. P. Alivisatos, "Colloidal nanocrystal shape and size control: the case of cobalt," *Science*, vol. 291, no. 5511, pp. 2115–2117, 2001.

[30] G. A. Sawatzky, J. M. D. Coey, and A. H. Morrish, "Mössbauer study of electron hopping in the octahedral sites of Fe_3O_4," *Journal of Applied Physics*, vol. 40, no. 3, pp. 1402–1403, 1969.

[31] G. A. Sawatzky, F. van der Woude, and A. H. Morrish, "Mössbauer study of several ferrimagnetic spinels," *Physical Review*, vol. 187, no. 2, pp. 747–757, 1969.

[32] A. N. Zakharov, E. A. Gan'shina, N. S. Perov, N. I. Yurasov, and A. Y. Shenkarenko, "Opal photonic crystals modified by Fe-based inclusions," *Inorganic Materials*, vol. 41, no. 11, pp. 1185–1188, 2005.

[33] R. Grau-Crespo, A. Y. Al-Baitai, I. Saadoune, and N. H. De Leeuw, "Vacancy ordering and electronic structure of γ-Fe_2O_3 (maghemite): a theoretical investigation," *Journal of Physics Condensed Matter*, vol. 22, no. 25, Article ID 255401, 2010.

[34] K. J. Davies, S. Wells, R. V. Upadhyay et al., "The observation of multi-axial anisotropy in ultrafine cobalt ferrite particles used in magnetic fluids," *Journal of Magnetism and Magnetic Materials*, vol. 149, no. 1-2, pp. 14–18, 1995.

[35] N. Moume, P. Bonville, and M. P. Pileni, "Control of the size of cobalt ferrite magnetic fluids: Mössbauer spectroscopy," *The Journal of Physical Chemistry*, vol. 100, no. 34, pp. 14410–14416, 1996.

[36] L. Josephson, J. Lewis, P. Jacobs, P. F. Hahn, and D. D. Stark, "The effects of iron oxides on proton relaxivity," *Magnetic Resonance Imaging*, vol. 6, no. 6, pp. 647–653, 1988.

[37] T. Allkemper, C. Bremer, L. Matuszewski, W. Ebert, and P. Reimer, "Contrast-enhanced blood-pool MR angiography with optimized iron oxides: effect of size and dose on vascular contrast enhancement in rabbits," *Radiology*, vol. 223, no. 2, pp. 432–438, 2002.

[38] S. Gangopadhyay, G. C. Hadjipanayis, B. Dale et al., "Magnetic properties of ultrafine iron particles," *Physical Review B*, vol. 45, no. 17, pp. 9778–9787, 1992.

[39] J. Aizenberg, A. J. Black, and G. M. Whitesides, "Control of crystal nucleation by patterned self-assembled monolayers," *Nature*, vol. 398, no. 6727, pp. 495–498, 1999.

[40] S.-M. Lee, Y.-W. Jun, S.-N. Cho, and J. Cheon, "Single-crystalline star-shaped nanocrystals and their evolution: programming the geometry of nano-building blocks," *Journal of the American Chemical Society*, vol. 124, no. 38, pp. 11244–11245, 2002.

[41] X. Huang and Z. Chen, "Preparation of $CoFe_2O_4/SiO_2$ nanocomposites by sol-gel method," *Journal of Crystal Growth*, vol. 271, no. 1-2, pp. 287–293, 2004.

[42] J. Li, D. Dai, B. Zhao, Y. Lin, and C. Liu, "Properties of ferrofluid nanoparticles prepared by coprecipitation and acid treatment," *Journal of Nanoparticle Research*, vol. 4, no. 3, pp. 261–264, 2002.

[43] J. Araújo, E. Vega, C. Lopes, M. A. Egea, M. L. Garcia, and E. B. Souto, "Effect of polymer viscosity on physicochemical properties and ocular tolerance of FB-loaded PLGA nanospheres," *Colloids and Surfaces B*, vol. 72, no. 1, pp. 48–56, 2009.

[44] H.-S. Kim, W.-I. Park, M. Kang, and H.-J. Jin, "Multiple light scattering measurement and stability analysis of aqueous carbon nanotube dispersions," *Journal of Physics and Chemistry of Solids*, vol. 69, no. 5-6, pp. 1209–1212, 2008.

[45] D. Desai, S. Kothari, and M. Huang, "Solid-state interaction of stearic acid with povidone and its effect on dissolution stability of capsules," *International Journal of Pharmaceutics*, vol. 354, no. 1-2, pp. 77–81, 2008.

[46] S. Ikeda, K. Miura, H. Yamamoto et al., "A perpendicular-anisotropy CoFeB-MgO magnetic tunnel junction," *Nature Materials*, vol. 9, no. 9, pp. 721–724, 2010.

[47] P. Gillis, F. Moiny, and R. A. Brooks, "On T_2-shortening by strongly magnetized spheres: a partial refocusing model," *Magnetic Resonance in Medicine*, vol. 47, no. 2, pp. 257–263, 2002.

[48] I. Prigogine and S. A. Rice, *Advances in Chemical Physics*, vol. 98, Wiley, New York, NY, USA, 1997.